Evaluation of Large-Scale Forcing during TOGA COARE for Cloud-Resolving Models and Single-Column Models

XIAOQING WU AND MITCHELL W. MONCRIEFF

National Center for Atmospheric Research,* Boulder Colorado

KERRY A. EMANUEL

Program for Atmospheres, Oceans, and Climate, Massachusetts Institute of Technology, Cambridge, Massachusetts

ABSTRACT

A moist enthalpy analysis is conducted to evaluate the large-scale forcing during the Tropical Ocean Global Atmosphere Coupled Ocean–Atmosphere Response Experiment. Two physically distinct periods are chosen, namely, a convectively disturbed period (19–24 December 1992) and an undisturbed period (7–12 January 1993). The predicted enthalpy is underestimated during the disturbed period but is closer to the observed value during the undisturbed period. The enthalpy is more sensitive to estimated errors in the large-scale forcing than to the radiative flux and surface heat flux during these two periods as well as during the entire 4-month period (1 November 1992–28 February 1993). The objective analyses used in estimates of large-scale forcing can strongly affect the prediction of enthalpy, especially during the period of strong convective precipitation.

1. Introduction

Much effort has been put into quantifying the large-scale role of cloud systems by employing finescale numerical models or cloud-resolving models (CRMs). By definition, this class of model simulates cloud-scale and mesoscale dynamics and its interaction with the mean flow in an explicit way. A primary strategic objective is to improve convective parameterization through advancing our basic understanding of the physics of cloud systems and their multiscale interactions. This longstanding problem concerns the collective effects of cloud systems rather than the detailed influence of any one process (i.e., microphysics, turbulence, surface fluxes, or radiation).

The intensive observing periods conducted during major field campaigns provide independent datasets with which to evaluate the simulated cloud-scale and mesoscale response to large-scale forcing. These datasets include satellite-measured radiative fluxes, surface heat fluxes, and radar-derived rainfall data, among others. Moreover, the large-scale observations and the validated synthetic cloud-scale results available from the numerical simulations together provide a valuable dataset for quantifying the transport properties of convection and its interaction with the large-scale flow.

Despite successful simulations of the long-term behavior of tropical cloud systems in the Global Atmospheric Research Programme (GARP) Atlantic Tropical Experiment and the Tropical Ocean Global Atmosphere (TOGA) Coupled Ocean–Atmosphere Response Experiment (COARE) using the CRM approach, biases in the simulated temperature and moisture fields are revealed by making comparisons with observations (e.g., Grabowski et al. 1996; Xu and Randall 1996; Wu and Moncrieff 1996; Wu et al. 1998). In particular, Wu et al. (1998) showed that during 7–12 January 1993 (toward the end of the 39-day simulation in TOGA COARE), the model-produced temperature and moisture fields are too warm and too moist. The temperature and moisture biases also occurred in three-dimensional cloud-resolving simulations (e.g., Wu and Moncrieff 1996; Grabowski et al. 1998). The CRMs and single-column models involved in the Global Energy and Water Cycle Experiment (GEWEX) Cloud System Study Working Group 4 intercomparison project showed that a cold bias occurred during the simulated 6-day period (19–24 December 1992), which was distinguished by strong con-

---

Corresponding author address: Dr. Xiaoqing Wu, NCAR, P.O. Box 3000, Boulder, CO 80307.
E-mail: xiaoqing@ucar.edu

vective activity and attendant large-scale forcing (Krueger 1996; Moncrieff et al. 1997).

Because the biases are common to several CRMs employing a range of numerical techniques, it can be assumed that they are of physical origin rather than a numerical artifact. The model physics (by which we mean a combination of parameterized processes and resolved-scale transport) and the large-scale forcing are two primary candidate explanations. A key uncertainty springs from the effect of processes that cannot be resolved even in CRMs, particularly rates of change among the three phases of water, turbulent processes in the boundary layer and at the surface, and solar and longwave radiation. The microphysical parameterizations are arguably the most uncertain in long-term simulations, considering that computational limitations compel the use of simple bulk parameterizations (ice and liquid phases), which are not necessarily physically based. In fact, Wu et al. (1999) showed that the CRM, with modified ice phase processes based on certain field measurements, did produce smaller temperature and moisture biases. While uncertainties in microphysical parameterizations receive most attention, the subgrid-scale physics of the turbulent planetary boundary layer is equally uncertain. Some of these uncertainties will be alleviated when computer power progressively allows boundary layer features in CRM simulations, for example, eddies of characteristic scale comparable to the depth of the boundary layer, to be better resolved.

While the model physics is a prime candidate, the imposed large-scale forcing for the temperature and moisture fields is another cause of bias. Recently, Emanuel and Živković-Rothman (1999) performed a moist enthalpy analysis for the 4-month TOGA COARE period to evaluate the quality of the large-scale forcing without recourse to CRMs or convection parameterization. Recognizing the need for accurate measurements of the radiative fluxes at the surface and at the top of the atmosphere (TOA) and surface heat fluxes in the enthalpy analysis, they argued that the errors in the imposed large-scale forcing for temperature and moisture fields are the primary source of bias.

We perform a moist enthalpy analysis of two meteorologically distinct periods; namely, a convectively disturbed period (19–24 December 1992) and a relatively undisturbed period (7–12 January 1993). In view of the uncertainties in the radiative flux and the surface heat flux, one observed and two model-produced estimates of radiative and surface fluxes are used. The moist enthalpy analysis is also performed for the entire period of TOGA COARE (1 November 1992–28 February 1993) using the large-scale forcing obtained from two different analysis techniques. The objective is to understand the uncertainty caused by large-scale forcing. In the next section we describe the procedure of moist enthalpy analysis. The datasets used are described in section 3, followed in section 4 by a presentation of the results and, finally, a discussion in section 5.

2. Moist enthalpy analysis

Following Emanuel (1994), the moist enthalpy can be written as

$$k = (C_{pd} + C_l q_t)T + L_v q_v - L_f q_i, \qquad (1)$$

where T is the temperature, q_v the water vapor mixing ratio, q_i is the ice water mixing ratio; q_t ($=q_v + q_l + q_i$) the total water mixing ratio, and q_l the liquid water mixing ratio. The C_{pd} is the heat capacity at constant pressure for dry air, C_l the heat capacity of liquid water, L_v the latent heat of vaporization, and L_f the latent heat of fusion. Note that the moist enthalpy (and water vapor mixing ratio) is used in this study, while the moist specific enthalpy (and specific humidity) is used in Emanuel and Živković-Rothman (1999).

Employing the conservation equations for the temperature and moisture, the global moist enthalpy conservation equation is

$$\int_{P_t}^{P_s} \left[(C_{pd} + C_l q_t)\left(\frac{\partial T}{\partial t} + \mathbf{v} \cdot \nabla T + \omega \frac{\partial T}{\partial p}\right) - \alpha\omega + \frac{\partial(L_v q_v)}{\partial t} + \mathbf{v} \cdot \nabla(L_v q_v) + \omega\frac{\partial(L_v q_v)}{\partial p} \right] dp$$

$$= H_T = H_{q_v} + R_{\text{SRF}} - R_{\text{TOA}}, \qquad (2)$$

where H_T and H_{q_v} are the surface sensible and latent heat fluxes, respectively; R_{SRF} and R_{TOA} are the net radiative fluxes at the surface and at the TOA, respectively; $\mathbf{v}$ the horizontal vector velocity; ω the pressure velocity; α the volume per unit mass of air; p_s the surface pressure (1008 hPa used in the analysis) and p_t the pressure at the top of the column (50 hPa).

Rearranging Eq. (2), the time change of vertically integrated moist enthalpy can then be approximated as

$$\frac{\partial}{\partial t} \int_{P_t}^{P_s} k \, dp = f_T + f_{q_v} + H_S + H_R, \qquad (3)$$

where

$$f_T = -\int_{p_t}^{p_s} \left[(C_{pd} + C_l q_t)\left(\mathbf{v} \cdot \boldsymbol{\nabla}T + \omega\frac{\partial T}{\partial p} \right) - \alpha\omega \right] dp$$

$$f_{q_v} = -\int_{p_t}^{p_s} \left[\mathbf{v} \cdot \boldsymbol{\nabla}(L_v q_v) + \omega\frac{\partial(L_v q_v)}{\partial p} \right] dp$$

$$H_S = H_T + H_{q_v}$$

$$H_R = R_{\mathrm{SRF}} - R_{\mathrm{TOA}}.$$

Variables f_T and f_{q_v} are the vertically integrated large-scale advective tendency (or forcing) for the temperature and the water vapor mixing ratio, respectively; H_S is the sum of surface sensible and latent heat fluxes; and H_R the radiative heating defined as the difference between radiative fluxes at the surface and TOA. The vertically integrated $C_l T \partial q_t / \partial t$ and $\mathbf{v} \cdot \boldsymbol{\nabla}(L_f q_i) + \omega \partial(L_f q_i)/\partial p$ are neglected.

3. Datasets

The two objectively analyzed TOGA COARE sounding datasets of Lin and Johnson (1996, hereafter LJ) and Ciesielski et al. (1997, hereafter CJ) were used to calculate f_T and f_{q_v}. The former, based on the iterative weighted-average interpolation scheme of Barnes (1964), has been used in month-long cloud-resolving simulations (Wu et al. 1998, 1999). The latter employed the multiquadric interpolation scheme of Nuss and Titley (1994) and was used in the single-column modeling of Emanuel and Živković-Rothman (1999). The evolving large-scale advective tendencies of temperature and moisture represent averages over the Intensive Flux Array (IFA) of TOGA COARE.

The observed surface latent and sensible heat fluxes are averages of the single improved meteorological (IMET) surface mooring and the three TOGA Tropical Atmosphere–Ocean Automated Temperature Line Acquisition System moorings. The radiative fluxes at the top of atmosphere are estimated from the flux and cloud (FC) dataset, which is derived from a radiative transfer model using the satellite-measured radiance and the cloud properties obtained from the International Satellite Cloud Climatology Project (Zhang et al. 1995). The surface radiative fluxes are measured from three ships (R/V *Kexue 1,* R/V *Shiyan 3,* and *Xiangyanghong 5*) and IMET buoy within the IFA.

Considering the uncertainties in the measurements of fluxes (e.g., Emanuel and Živković-Rothman 1999; Johnson and Ciesielski 2000), the CRM produced surface heat fluxes and radiative fluxes are also used; namely, the 39-day (5 December 1992–12 January 1993) simulation M0 presented in Wu et al. (1999). Two 6-day simulations are also performed for the disturbed period 19–24 December 1992 (S1) and the undisturbed period 7–12 January 1993 (W1), respectively. The design of the S1 and W1 experiments is the same as M0, except

that S1 starts from 0000 UTC 19 December 1992, and W1 from 0000 UTC 7 January 1993.

Observed condensate data (q_l and q_i) are unavailable because no direct observations of these quantities were made. Therefore, the vertically integrated moist enthalpy is calculated by Eq. (1) using q_v instead of q_t, for convenience henceforth referred to as the observed enthalpy (k_o). Nevertheless, the vertically integrated q_l and q_i are much smaller than the vertically integrated q_v. The vertically integrated moist enthalpy can also be obtained by integrating Eq. (3) using the large-scale forcing, surface heat fluxes, and radiative fluxes. This is referred to as the predicted enthalpy (k_p).

4. Results

a. Six-day moist enthalpy analysis

Figure 1a shows the evolution of the observed enthalpy (k_o) and three predicted enthalpies (k_p) for the convectively disturbed period using the LJ dataset. The observed enthalpy features little variability during the 6-day period; however, the predicted enthalpies gradually decrease from about 281 to 276 K. The enthalpies predicted using three different surface heat fluxes and radiative fluxes show a similar evolution. The difference between the observed and predicted enthalpy is about 5 K at the end of the 6-day period. Similar features are also present in the enthalpy analysis using the CJ dataset (Fig. 1b). The difference between the observed and predicted enthalpy at the end of the 6-day period is about 1 K larger than that in Fig. 1a.

The predicted enthalpies over the undisturbed period corresponding to the LJ and CJ datasets have different characteristics (Fig. 2). The predicted enthalpy using the LJ dataset is larger than the observed (Fig. 2a), while the one using the CJ dataset is smaller (Fig. 2b). In contrast to the disturbed period, the difference between the observed and predicted enthalpies is smaller during the undisturbed period.

To comprehend these differences, the evolution of each term on the right-hand side of Eq. (3) is plotted for the disturbed period (Fig. 3) and for the undisturbed period (Fig. 4). The vertically integrated large-scale advective tendencies in Figs. 3a and 4a are the sum of f_T and f_{q_v}. During the disturbed period, the large-scale advective tendency contributes a net cooling (Fig. 3a). The 6-day mean forcing is -1.84 K day^{-1} for the LJ dataset and -2.03 K day^{-1} for the CJ dataset, which explains why the predicted enthalpy is smaller using CJ than LJ. For the most part, the radiative heating from S1 and M0 agrees with the observed radiative heating, which shows strong diurnal variability (Fig. 3b). The 6-day mean radiative heating is -0.33 K day^{-1} for observations (OB), -0.36 K day^{-1} for M0, and -0.43 K day^{-1} for S1. Moreover, the surface heat fluxes from S1 and M0 are consistent with the observed surface heat fluxes, which contribute a net warming (Fig. 3c). The
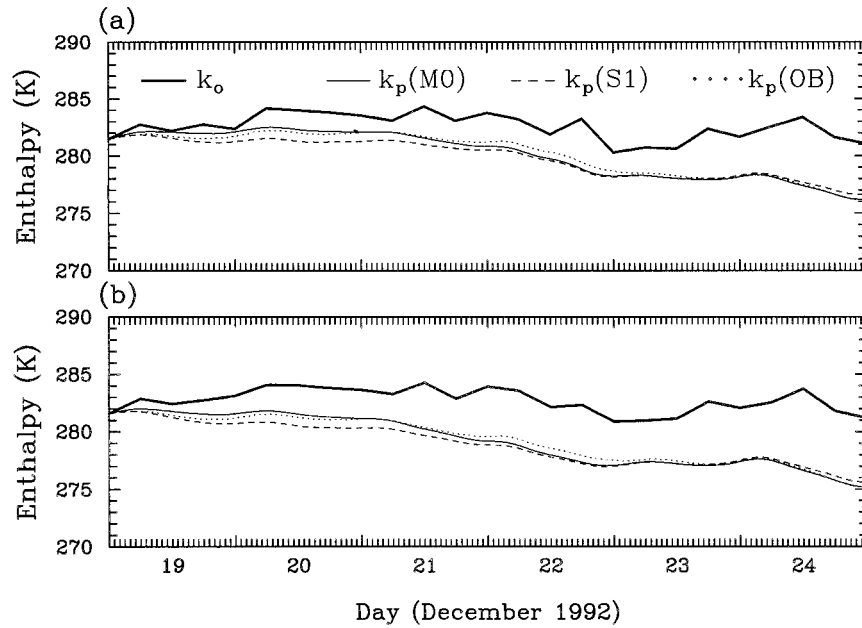
FIG. 1. Evolution of the 6-hourly observed enthalpy (k_o) and the predicted enthalpy (k_p) divided by $C_{pd} \times 958$ hPa for (a) the LJ analysis and (b) the CJ analysis during the disturbed period. The vertically integrated enthalpy is divided by the heat capacity of the troposphere C_{pd}. Here, OB means the indirectly observed FC radiative heating and observed surface flux data are used to calculate the enthalpy with Eq. (3), while M0 and S1 indicate that the model-produced radiative heating and surface flux data are used.

6-day mean heat flux is 1.29 K day^{-1} for OB, 1.32 K day^{-1} for M0, and 1.47 K day^{-1} for S1. The agreement between the observed and modeled surface heat fluxes and radiative heating leads to the three similar predicted enthalpies shown in Fig. 1a and Fig. 1b.

For the undisturbed period, the large-scale advective tendency contributes net warming in the first half, and net cooling during the second half, of the 6-day period (Fig. 4a). The 6-day mean forcing is 0.55 K day^{-1} for LJ and 0.31 K day^{-1} for CJ. The radiative heating ob-
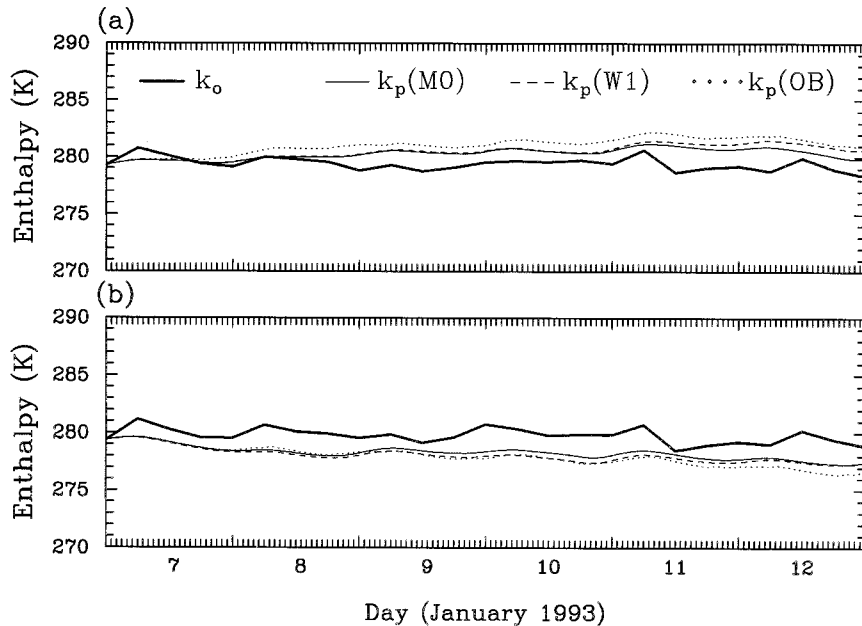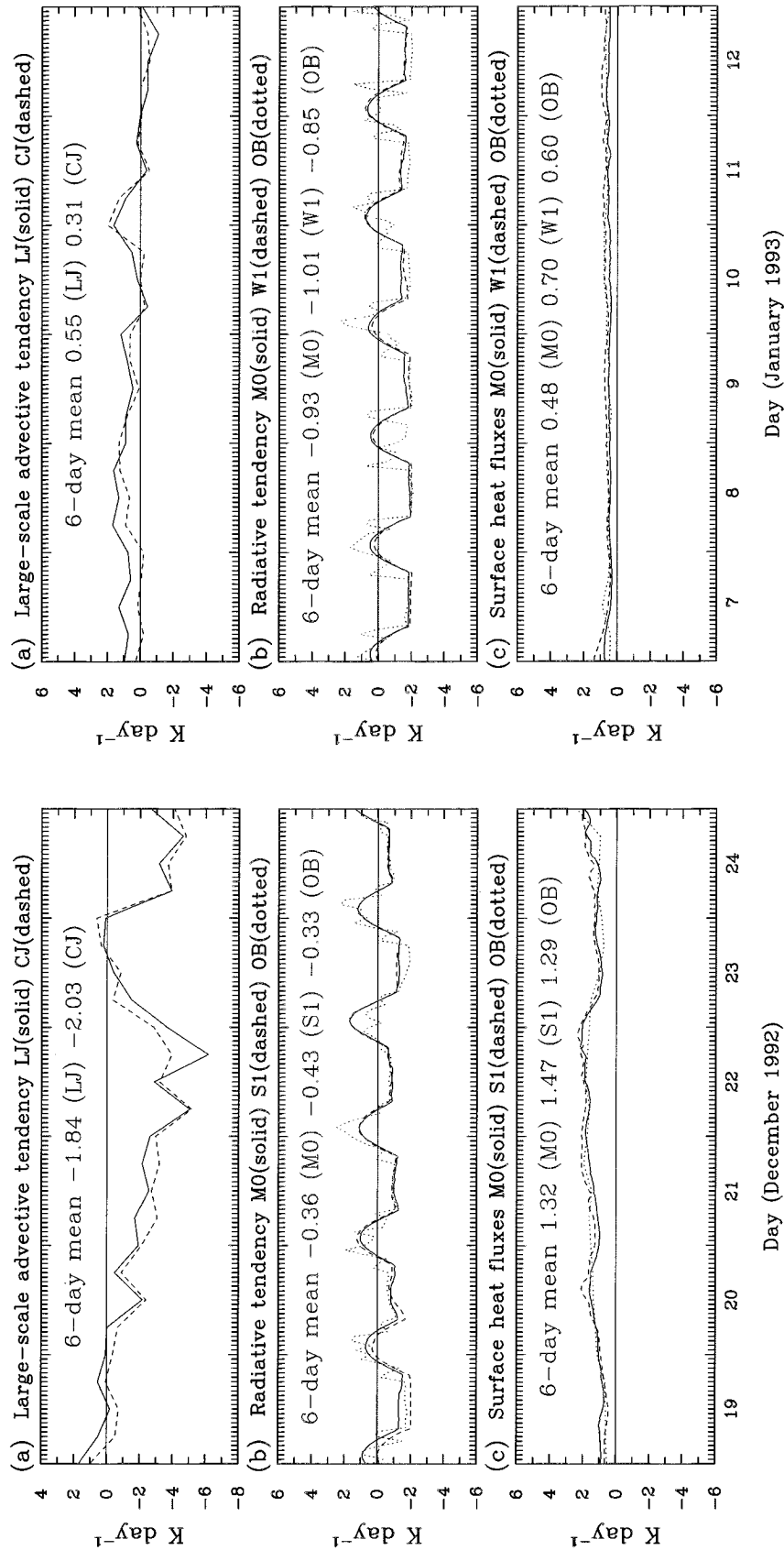

FIG. 2. Same as Fig. 1 but during the undisturbed period.

FIG. 3. Evolution of the 6-hourly (a) vertically integrated large-scale advective tendency of temperature and moisture, (b) vertically integrated radiative heating, and (c) surface heat fluxes for the disturbed period.
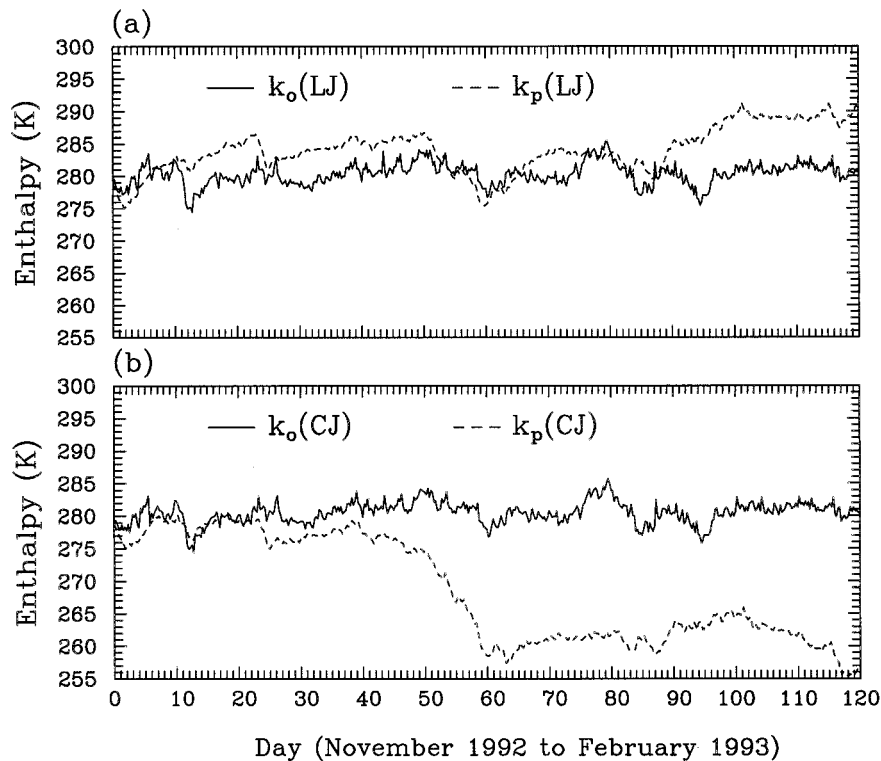
FIG. 4. Same as Fig. 3 but for the undisturbed period.

FIG. 5. The 120-day evolution of 6-hourly observed (k_o) and predicted (k_p) enthalpies divided by $C_{pd} \times 958$ hPa for (a) the LJ analysis and (b) the CJ analysis. A low-pass time filter with a 5-day cutoff period is applied in the time series (Ormsby 1961).

tained from the observation and the models is generally consistent. The nocturnal cooling is more pronounced in the observations than in the simulations (Fig. 4b). The respective 6-day mean radiative heating is -0.85 K day^{-1} for OB, -0.93 K day^{-1} for M0, and -1.01 K day^{-1} for W1. The surface heat fluxes from both the observation and models contribute a small net warming (Fig. 4c). The 6-day mean heat flux is 0.60 K day^{-1} for OB, 0.48 K day^{-1} for M0, and 0.70 K day^{-1} for W1.

A pertinent point is that the predicted enthalpies are grouped mainly in terms of the forcing during both disturbed and undistubed periods. In other words, the predicted enthalpies are more sensitive to the advective forcing than to the radiative fluxes and surface heat fluxes.

b. Four-month moist enthalpy analysis

To further evaluate the large-scale forcing, we extend the enthalpy analysis to the entire 4-month period of TOGA COARE. Figures 5a and 5b show the 120-day evolution of observed (k_o) and predicted (k_p) enthalpies using the LJ and CJ datasets, respectively. A striking feature is the difference between the two predicted enthalpies. The k_p is generally larger than k_o for LJ (Fig. 5a), while the opposite is true for CJ (Fig. 5b). At the end of the 120-day period, $k_o - k_p$ is about -10 K for

LJ and 25 K for CJ, mainly caused by a rapid decrease of k_p for CJ between day 40 and day 60. This behavior is also evident in Emanuel and Živković-Rothman (1999), who used the CJ dataset.

Because the same radiative flux and surface heat flux are used to predict k_p for LJ and CJ, the large-scale forcing is the responsible factor (Fig. 6). For most of the 120-day period, the large-scale forcing for LJ is similar to that for CJ (Fig. 6a), apart from the large differences between days 40–70 and days 90–120. The difference of the 120-day mean forcing between LJ and CJ is about 0.3 K day^{-1} (30 W m^{-2}), which corresponds to a 35 K difference in predicted enthalpy at the end of the 120-day period.

The 120-day evolutions of radiative tendency and surface heat flux used in the enthalpy analysis are shown in Figs. 6b and 6c, respectively. The mean radiative tendency is -0.38 K day^{-1} (Fig. 6b), close to the budget-estimated value (-0.42 K day^{-1}) and other estimates (Johnson and Ciesielski 2000). This is somewhat surprising considering the uncertainties in the measurements and estimations. The 120-day mean surface heat flux is 0.99 K day^{-1} or 112.4 W m^{-2} (Fig. 6c), close to the 110.7 W m^{-2} derived from the Special Sensor Microwave/Imager (Chou et al. 1997).

Figures 5a and 5b suggest that the time change of $k_o - k_p$ better identifies the difference between the pre-
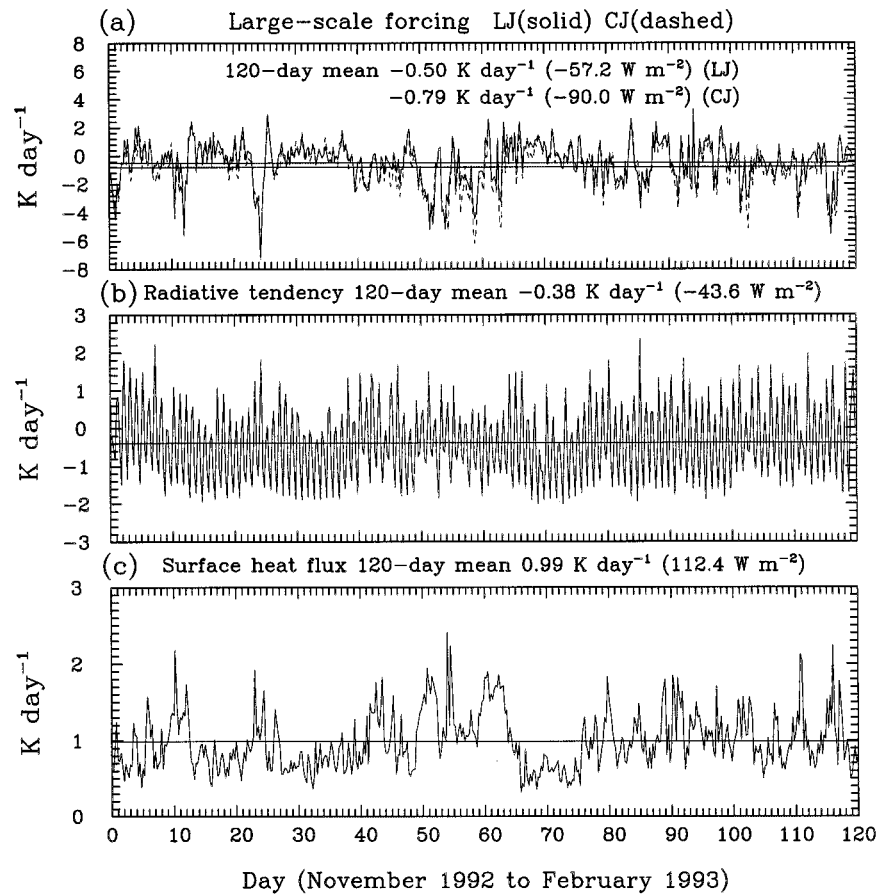
FIG. 6. The 120-day evolution of the 6-hourly (a) vertically integrated large-scale advective tendency of temperature and moisture, (b) vertically integrated radiative heating, and (c) surface heat fluxes.

dicted and observed enthalpies. The evolution of $\partial(k_o - k_p)/\partial t$ is compared with the Geostationary Meteorological Satellite (GMS) brightness temperature (TBB) in Fig. 7. A low-pass filter with a 5-day cutoff period is applied to the time series. The evolutions of $\partial(k_o - k_p)/\partial t$ are similar for LJ (solid line) and CJ (dashed line), but compared to LJ, CJ has larger positive values be-

tween days 40–70 and days 90–120. Positive values of $\partial(k_o - k_p)/\partial t$ are associated with the colder (negative) TBB, which is due to the deep convection and cold cloud tops, while negative values are related to the warmer (positive) TBB. This result is further evidence that the forcing may be overestimated during the period of strong convective precipitation (Johnson and Ciesielski 2000).
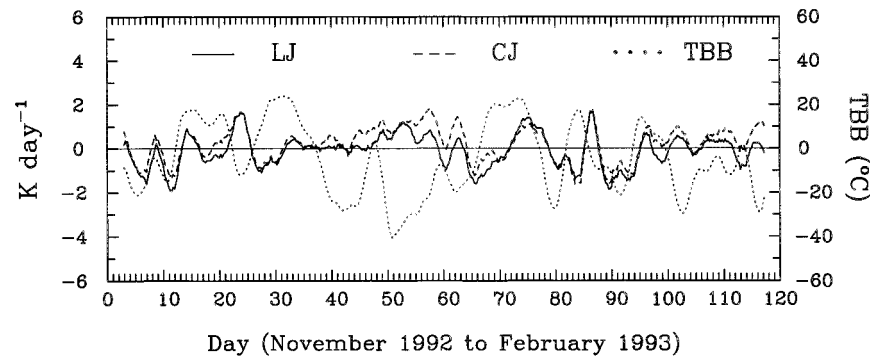

FIG. 7. Evolution of 5-day low-pass filtered $\partial(k_o - k_p)/\partial t$ for the LJ dataset (solid line) and CJ dataset (dashed line), and the GMS brightness temperature (TBB) (dotted line).
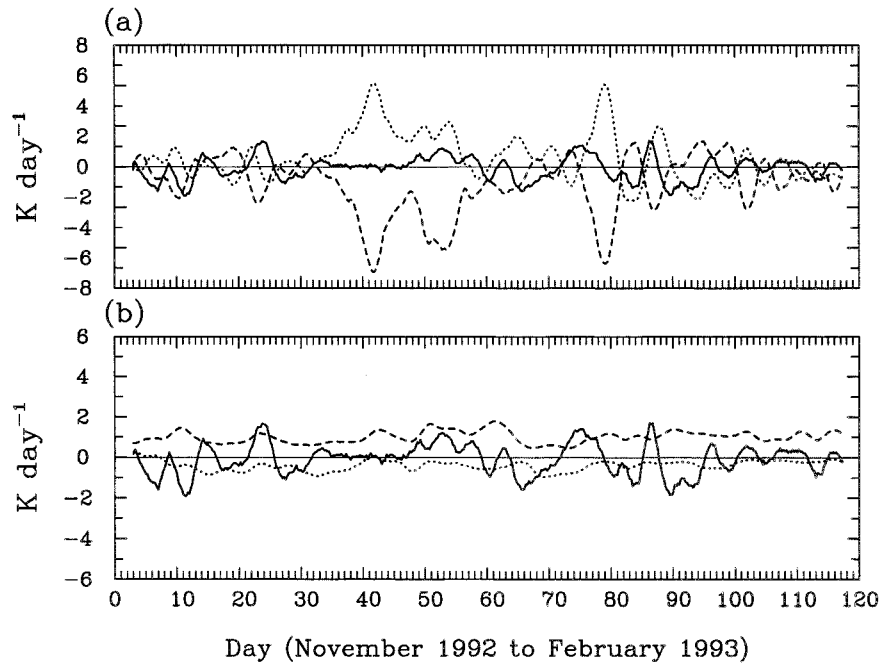
FIG. 8. Evolution of 5-day low-pass filtered $\partial(k_o - k_p)/\partial t$ (solid lines in both panels): (a) f_T (dashed line) and f_{q_v} (dotted line), (b) H_S (dashed line) and H_R (dotted line) for the LJ dataset.

The evolution of $\partial(k_o - k_p)/\partial t$ is compared with the observed temperature and moisture forcing (Fig. 8a) and with the observed surface heat flux and radiative heating (Fig. 8b), respectively, for the LJ dataset. The correlation coefficients between $\partial(k_o - k_p)/\partial t$ and f_T, f_{q_v}, H_S, and H_R are -0.35, 0.20, 0.03, and -0.09, respectively. Similar relationships are also found for the CJ dataset. This indicates that the predicted enthalpy bias is better correlated with the observed temperature and moisture forcing than with the radiative and surface heat fluxes.

5. Discussion

Uncertainties in both model physics and large-scale forcing are two primary reasons for the temperature and moisture biases that occur in cloud-resolving models and single-column models. Uncertainties arising from model physics have been proposed as a result of CRM studies. The causes of the bias include the lack of large-scale advection of liquid and ice condensate (Grabowski et al. 1996; Wu et al. 1998); the effect of convective organization on the surface fluxes, which affects the energy and moisture supply at mesoscales (Tao et al. 1999); and the effect of ice microphysical parameterization (Wu et al. 1999). The uncertainty arising from forcing was proposed by Emanuel and Živković-Rothman (1999) on the basis of a moist enthalpy analysis.

To quantify the forcing issue, 6-day and 120-day moist enthalpy analyses were performed using two objectively analyzed datasets. We find that the predicted enthalpy is more sensitive to the large-scale forcing than to the radiative flux and surface heat flux. The difference between the predicted and observed enthalpies during the strongly disturbed period, when the large-scale forcing is the dominant term, is larger than that during the undisturbed period. The underprediction of enthalpy in the disturbed case is primarily due to the overestimation of the large-scale forcing. Johnson and Ciesielski (2000) proposed several likely causes for the overestimation of the forcing. These include the effect of rain on the computation of vertical velocity and errors in the humidity field.

In order to conserve enthalpy, Emanuel and Živković-Rothman (1999) applied a 40% correction to the forcing by adjusting the vertical velocity, and 60% by modifying the radiative flux. However, our analysis suggests that the change of forcing alone can result in a better prediction of enthalpy. Additional enthalpy analysis using the datasets produced by different objective analysis schemes such as the successive correction scheme (Daley 1991; Tung et al. 1999) and the variational scheme (Zhang and Lin 1997) should give more insight. By default, the variational scheme satisfies enthalpy conservation but requires accurate measurements of the area-integrated precipitation, surface heat flux, and radiative flux.

REFERENCES

Barnes, S. L., 1964: A technique for maximizing details in numerical weather map analysis. *J. Appl. Meteor.,* **3,** 396–409.

Chou, S.-H., C.-L. Shie, R. M. Atlas, and J. Ardizzone, 1997: Air–sea fluxes retrieved from special sensor microwave imager data. *J. Geophys. Res.,* **102,** 12 705–12 726.

Ciesielski, P. E., L. M. Hartten, and R. H. Johnson, 1997: Impacts of merging profiler and rawinsonde winds on TOGA COARE analyses. *J. Atmos. Oceanic Technol.,* **14,** 1264–1279.

Daley, R., 1991: *Atmospheric Data Analysis.* Cambridge University Press, 457 pp.

Emanuel, K. A., 1994: *Atmospheric Convection.* Oxford University Press, 580 pp.

——, and M. Živković-Rothman, 1999: A convection scheme for use in climate models. Part I: Development and evaluation. *J. Atmos. Sci.,* **56,** 1766–1782.

Grabowski, W. W., X. Wu, and M. W. Moncrieff, 1996: Cloud-resolving modeling of tropical cloud systems during Phase III of GATE. Part I: Two-dimensional experiments. *J. Atmos. Sci.,* **53,** 3684–3709.

——, ——, ——, and W. D. Hall, 1998: Cloud-resolving modeling of cloud systems during phase III of GATE. Part II: Effects of resolution and the third spatial dimension. *J. Atmos. Sci.,* **55,** 3264–3282.

Johnson, R. H., and P. E. Ciesielski, 2000: Rainfall and radiative heating rates from TOGA COARE atmospheric budgets. *J. Atmos. Sci.,* **57,** 1497–1514.

Krueger, S. K., 1996: A GCSS intercomparison of cloud-resolving models based on TOGA COARE observations. *Workshop Proc. New Insights and Approaches to Convective Parameterization,* Reading, United Kingdom, ECMWF, 113–127.

Lin, X., and R. H. Johnson, 1996: Kinematic and thermodynamic characteristics of the flow over the western Pacific warm pool during TOGA COARE. *J. Atmos. Sci.,* **53,** 695–715.

Moncrieff, M. W., S. K. Krueger, D. Gregory, J.-L. Redelsperger, and W.-K. Tao, 1997: GEWEX Cloud System Study (GCSS) Working Group 4: Precipitating convective cloud systems. *Bull. Amer. Meteor. Soc.,* **78,** 831–845.

Nuss, W. A., and D. W. Titley, 1994: Use of multiquadric interpolation for meteorological objective analysis. *Mon. Wea. Rev.,* **122,** 1611–1631.

Ormsby, J. F. A., 1961: Design of numerical filters with applications to missile data processing. *J. Assoc. Comput. Mach.,* **8,** 440–466.

Tao, W.-K., J. Simpson, C.-H. Sui, C.-L. Shie, B. Zhou, K. M. Lau, and M. W. Moncrieff, 1999: Equilibrium states simulated by cloud-resolving models. *J. Atmos. Sci.,* **56,** 3128–3139.

Tung, W.-W., C. Lin, B.Chen, M. Yanai, and A. Arakawa, 1999: Basic modes of cumulus heating and drying observed during TOGA-COARE IOP. *Geophys. Res. Lett.,* **26,** 3117–3120.

Wu, Xu., and M. W. Moncrieff, 1996: Recent progress on cloud-resolving modeling of TOGA COARE and GATE cloud systems. *Workshop Proc. New Insights and Approaches to Convective Parameterization,* Reading, United Kingdom, ECMWF, 128–156.

——, W. W. Grabowski, and M. W. Moncrieff, 1998: Long-term behavior of cloud systems in TOGA COARE and their interactions with radiative and surface processes. Part I: Two-dimensional modeling study. *J. Atmos. Sci.,* **55,** 2693–2714.

——, W. D. Hall, W. W. Grabowski, M. W. Moncrieff, W. D. Collins, and J. T. Kiehl, 1999: Long-term behavior of cloud systems in TOGA COARE and their interactions with radiative and surface processes. Part II: Effects of ice microphysics on cloud–radiation interaction. *J. Atmos. Sci.,* **56,** 3177–3195.

Xu, K.-M., and D. A. Randall, 1996: Explicit simulation of cumulus ensembles with the GATE Phase III data: Comparison with observations. *J. Atmos. Sci.,* **53,** 3710–3736.

Zhang, M. H., and J. L. Lin, 1997: Constrained variational analysis of sounding data based on column-integrated budgets of mass, heat, moisture, and momentum: Approach and application to ARM measurements. *J. Atmos. Sci.,* **54,** 1503–1524.

Zhang, Y.-C., W. B. Rossow, and A. A. Lacis, 1995: Calculation of surface and top of atmosphere radiative fluxes from physical quantities based on ISCCP datasets, 1. Method and sensitivity to input data uncertainties. *J. Geophys. Res.,* **100,** 1149–1165.